Supporting Information

Driving Electrochemical Oxygen Reduction and Hydrazine Oxidation Reaction by Enzyme-inspired Polymeric Cu(3,3'-Diaminobenzidine) Catalyst

Fei He[a], Li Mi[a], Yanfei Shen[b], Xinghua Chen[a], Yiran Yang[a], Hao Mei[a], Songqin Liu[a], Toshiyuki Mori[b] and Yuanjian Zhang*[a]

[a] Jiangsu Engineering Laboratory of Smart Carbon-Rich Materials and Device, Jiangsu Province Hi-Tech Key Laboratory for Bio-Medical Research, School of Chemistry and Chemical Engineering, Southeast University, Nanjing 211189, China

[b] Medical School, Southeast University, Nanjing 210009, China

[c]Global Research Center for Environment and Energy Based on Nanomaterials Science (GREEN), National Institute for Materials Sciences (NIMS), 1-1 Namiki, Ibaraki, 305-0044, Japan

(*) Email: Yuanjian.Zhang@seu.edu.cn

Table of contents

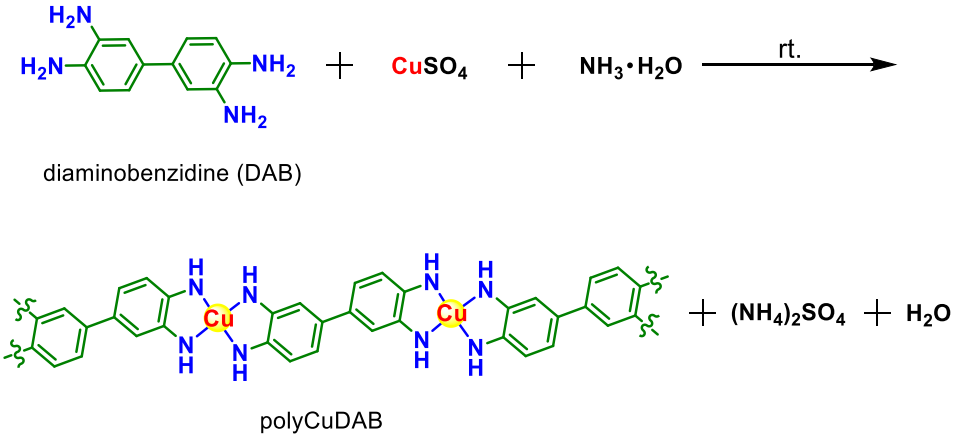

Scheme S1 The chemical reaction equation for synthesis of polyCuDAB. Depending on the ratio of diaminobenzidine (DAB) ligand to Cu^{2+}, up to four $-NH_2$ moieties can complex with one Cu ion.

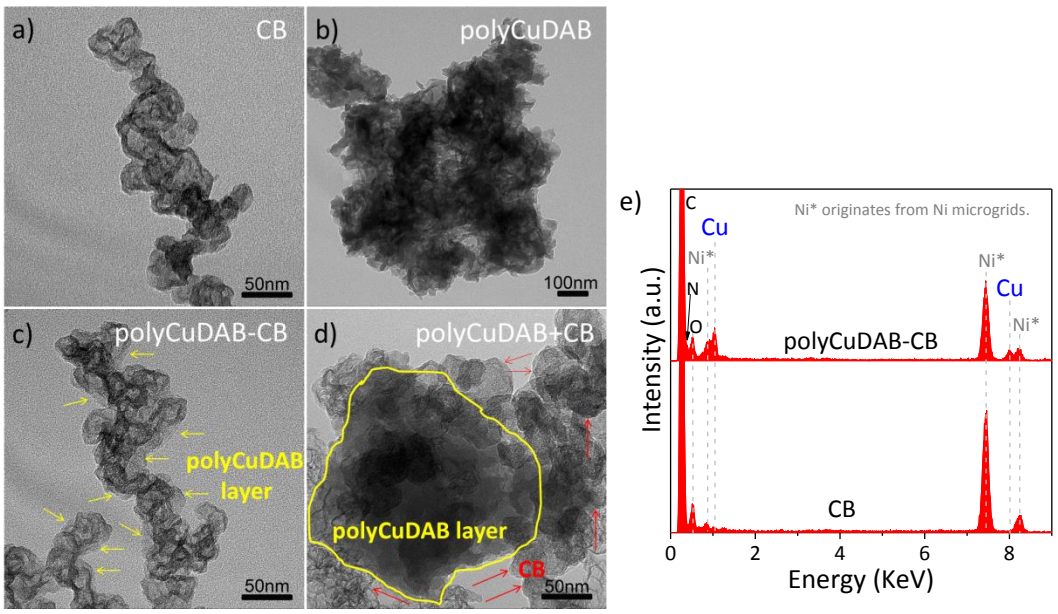

Figure S1 TEM images of CB (a), polyCuDAB (b), polyCuDAB-CB (c), polyCuDAB+CB (d) and EDS data of polyCuDAB-CB and CB (e). All of the samples were drop-casted onto a carbon-coated Ni microgrids for the TEM and EDS studies. The yellow arrows in (c) and line in (d) denote the polyCuDAB layer. The red arrows in (d) denotes CB.

TEM images showed that CB was agglomerate and mainly consisted of nanoparticles with sizes of ca. 50 nm (Figure S1a), while polyCuDAB was even more agglomerate (Figure S1b). Interestingly, for polyCuDAB-CB (Figure S1c), the CB size kept almost the same, but its edges were homogenously surrounded by a thin polyCuDAB layer (yellow arrows) which seemed slightly blur under the identical condition of TEM observation due to a lower conductivity. The EDS in Figure S1e further verified that additional Cu appeared in polyCuDAB-CB. Therefore, by pre-absorption of conjugated DAB on CB as the ligand and backbone, polyCuDAB could be formed on the surface of CB with further complexation with Cu ions. As a control, polyCuDAB+CB (Figure S1d) were also prepared by physical mixing of CB and pre-prepared polyCuDAB. In contrast, an evident phase separation of CB and polyCuDAB was observed in TEM image (Figure S1d), which was attributed to the strong tendency of self-aggregation for the long and rigid chains of pre-polymerized polyCuDAB. It demonstrated that the assembly sequence of DAB ligand, Cu ions on CB would greatly influence the immobilization of polyCuDAB on CB.

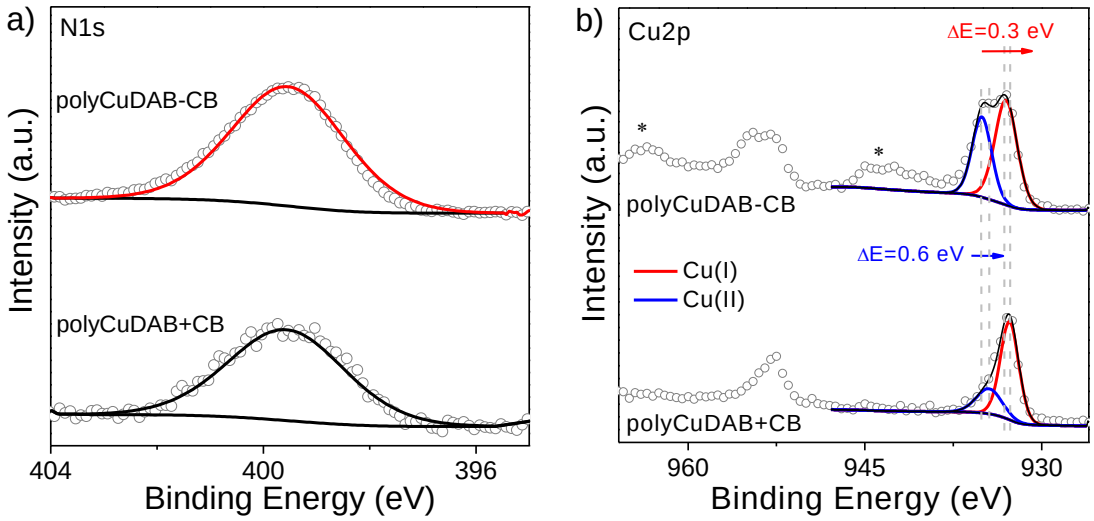

Figure S2 N1s and Cu2p XPS spectra of polyCuDAB+CB and polyCuDAB-CB. * in (b) represented the Cu2p satellite peaks.

Compared with polyCuDAB-CB, Cu2p XPS spectra of polyCuDAB+CB showed a negative peak shift, presumably attributing to the poorer π-π interaction and subsequently the less charge compensation by delocalized electron between polyCuDAB and CB in polyCuDAB+CB.

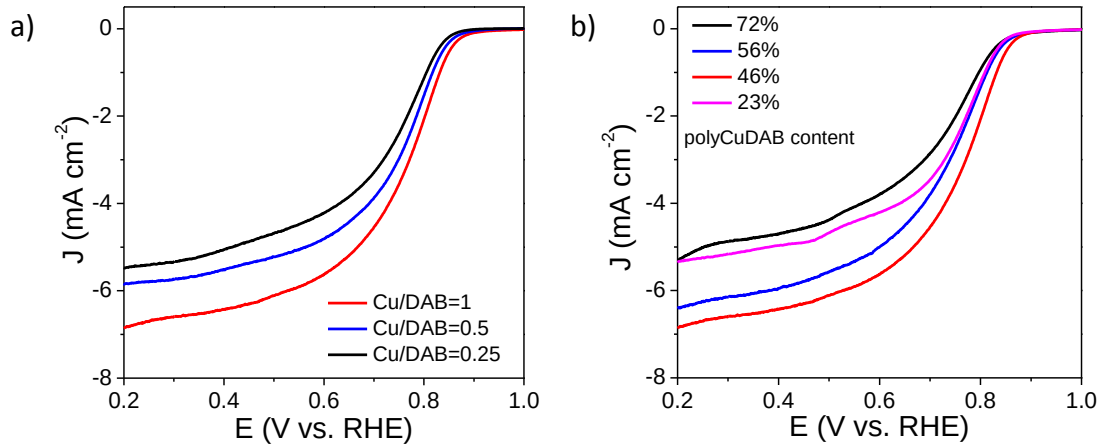

Figure S3 LSV curves of polyCuDAB-CB with different Cu/DAB ratio (a) and polyCuDAB loading (b) in O_2-saturated 0.1 M KOH.

It indicated that the polyCuDAB-CB with a loading of 46 wt.% and a Cu/DAB ratio of 1 (i.e. $–NH_2$/Cu=4) exhibited the best ORR performance.

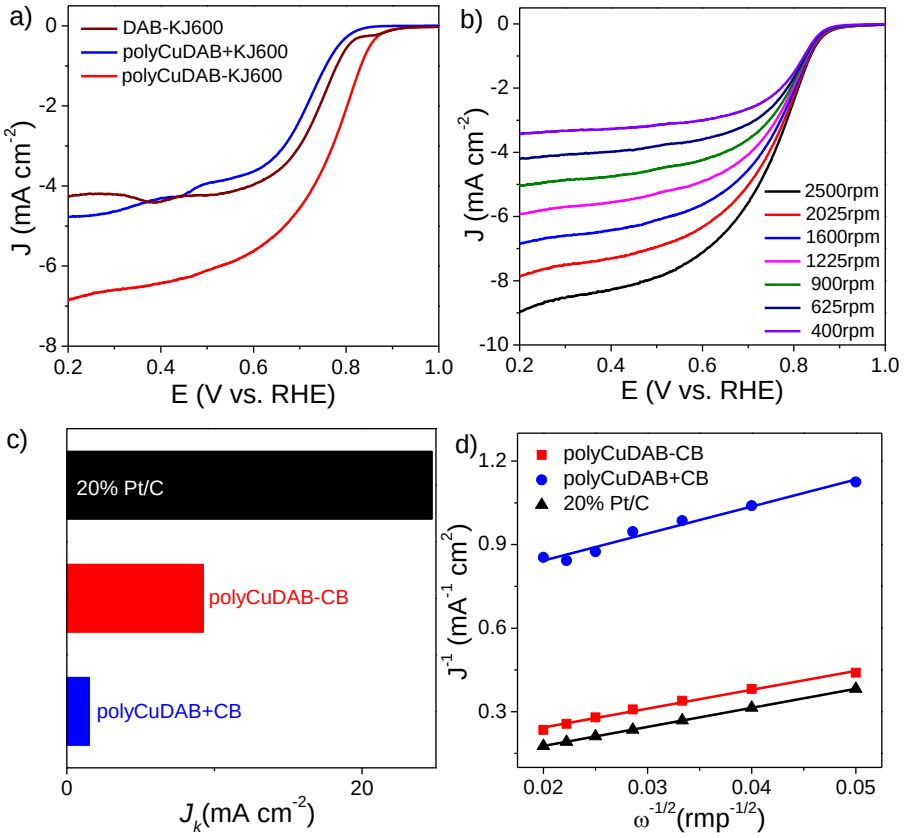

Figure S4 Comparison of ORR performance of DAB-CB, polyCuDAB+CB, polyCuDAB-CB and Pt/C. (a) LSV curves of DAB-CB, polyCuDAB+CB and polyCuDAB-CB in O_2-saturated 0.1 M KOH. (b) LSV curves of polyCuDAB-CB with different rotation rates. (c) J_k of different catalysts at 0.75 V. Sweep rate: 10 mV s^{-1}. (d) K-L plot (@0.75V) of 20% Pt/C, polyCuDAB+CB and polyCuDAB-CB.

E_{onset} and $E_{1/2}$ of polyCuDAB-CB (Figure S4a) showed a positive shift in comparison to DAB-CB, indicating Cu-N coordination could enhance the ORR activity. As a control, polyCuDAB+CB showed an inferior ORR performance, which suggested that tuning interfacial π-π stacking interaction also played a vital role in improving the ORR activity. In addition, polyCuDAB-CB exhibited the typical increasing current with higher rotations speeds (Figure S4b), indicating the ORR catalyzed by polyCuDAB-CB was a diffusion-controlled process.

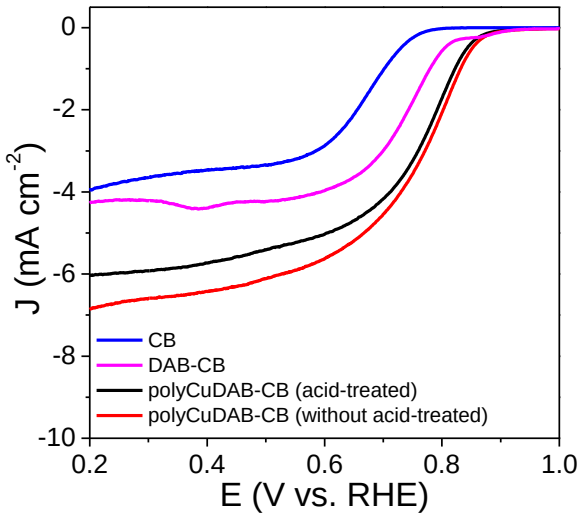

Figure S5 The effect of acid-treated process on the ORR activity of polyCuDAB-CB.

To exclude the possible effect of some impurities in for ORR, CB was pretreated by 6 M HCl solution for 24h at RT before use. Figure S5 showed that the ORR activity (E_{onset} and $E_{1/2}$) of polyCuDAB-CB (acid-treated) was still superior to that of CB and DAB-CB significantly, indicating that the possible promotion of catalytic activity from uncertain impurities in CB was negligible.

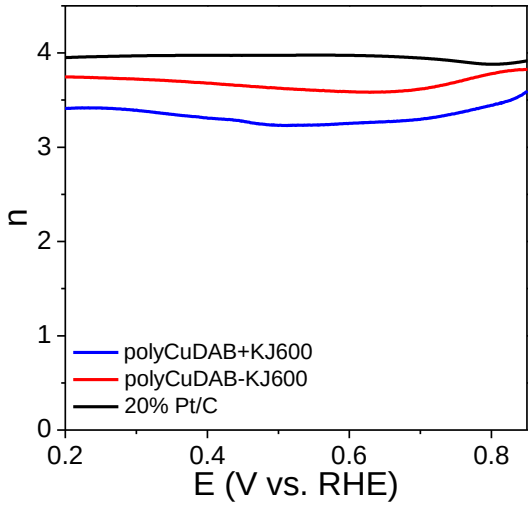

Figure S6 Electron transfer number of polyCuDAB+CB, polyCuDAB-CB, and Pt/C in ORR at different potentials.

The rotating ring-disk electrode (RRDE) measurements at 1600 rpm showed the electron-transfer number (n) of polyCuDAB-CB was 3.58-4.00 in the whole reduction potential region (Figure S6), indicating a nearly 4e reduction pathway, which was similar to that of Pt/C.

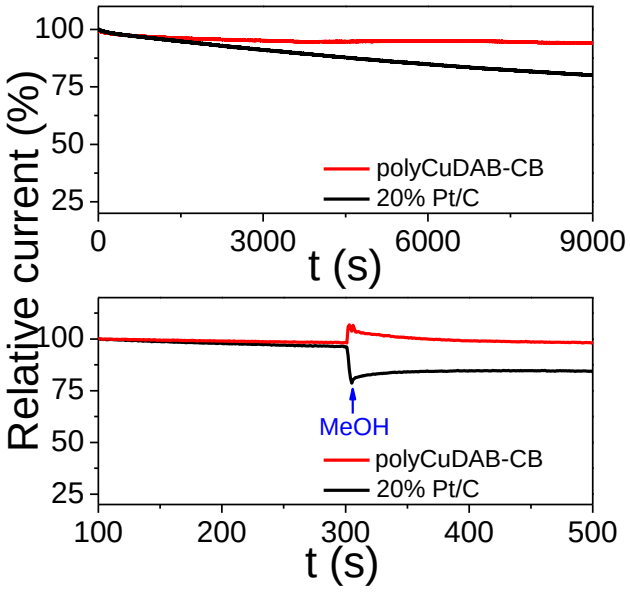

Figure S7 Current-time (I-t) responses and crossover effect evaluation of methanol oxidation of polyCuDAB-CB and 20% Pt/C. Biased potential: 0.565 V.

PolyCuDAB-CB showed high stability and little crossover from methanol oxidation as compared to Pt/C.

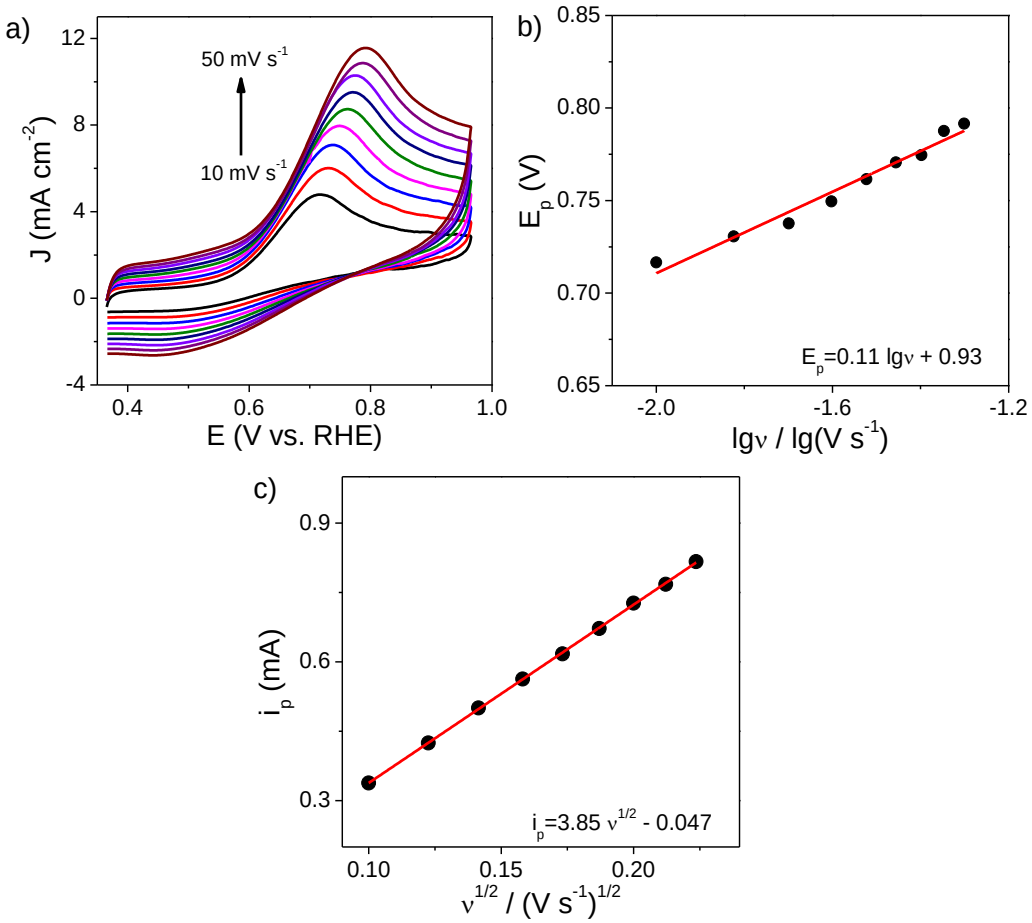

Figure S8 a) CVs of polyCuDAB-CB in 0.1 M KOH containing 10 mM hydrazine at various scan rates. b) The dependence of the peak current (i_p) on the square root of the scan rate ($\nu^{1/2}$). c) The dependence of the peak potential (E_p) on the natural logarithm of the scan rate ($lg\nu$).

The peak potentials (E_p) shifted positively with increasing ν, indicating HOR on polyCuDAB-CB was an irreversible process (E_p=0.11$lg\nu$ + 0.93). The linear relationship between the anodic peak current (i_p) and the square root of scan rate ($\nu^{1/2}$) demonstrated that HOR on polyCuDAB-CB was a diffusion-limited process (i_p=3.85$\nu^{1/2}$ – 0.047).

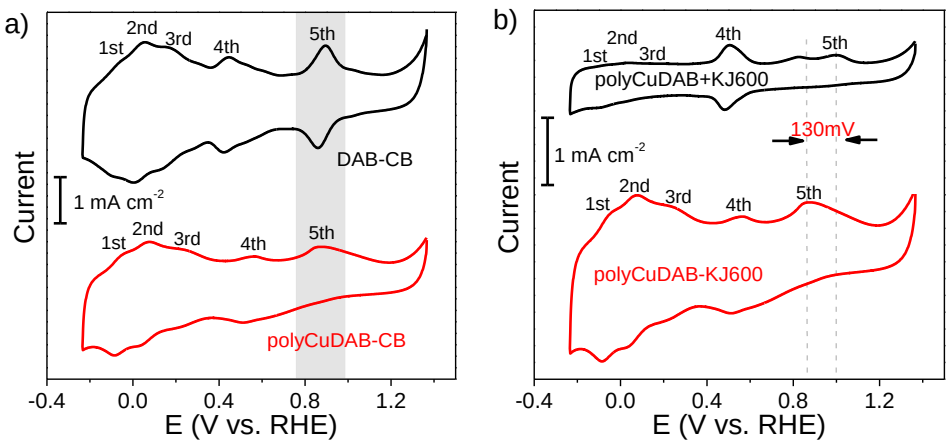

Figure S9 CV curves of DAB-CB, polyCuDAB+CB and polyCuDAB-CB in N_2-saturated 0.1 M KOH.

As shown in Figure S9a, DAB-CB exhibited five pairs of redox waves in N_2-saturated 0.1 M KOH, essentially showing its potential in delivering electrons in ORR. After complexing of DAB with Cu, the former four redox peaks of polyCuDAB-CB showed a positive shift compared with that of DAB-CB. Additionally, the fifth pair of redox wave in polyCuDAB-CB, which was supposed to correlate with the Cu(II)/Cu(I)-N complex center redox transition accompanying with the adsorption of OH^-,[1] became nearly irreversible. These results indicated that the electronic structure of π-conjugated DAB ligand was significantly altered in polyCuDAB-CB. As a control, the fifth pair of redox wave in polyCuDAB+CB positively shifted by 130 mV (Figure S9b), indicative of a poorer adsorption of OH^- and Cu-OH bond formation.

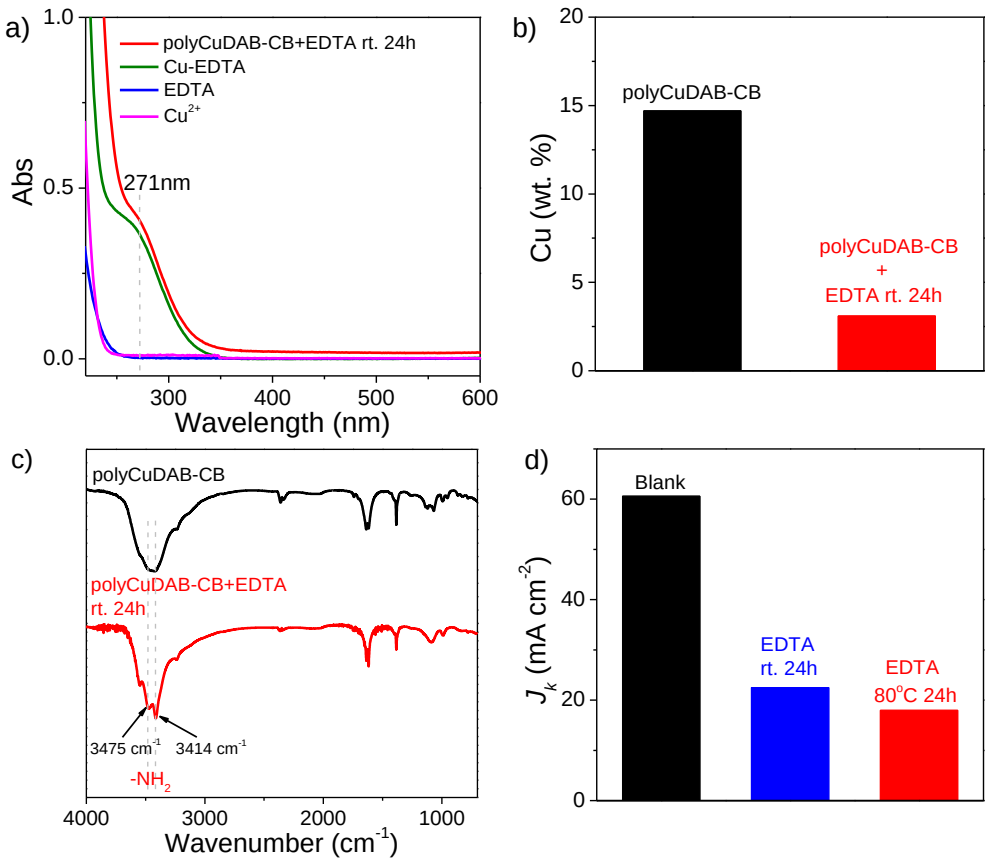

Figure S10 *Ex-situ* EDAT poisoning experiment of polyCuDAB-CB. (a) UV-vis spectra of Cu^{2+} ($Cu(NO_3)_2$ solution), EDTA, Cu-EDTA and the supernatant solution of EDTA poisoned polyCuDAB-CB. (b) Cu content in polyCuDAB-CB before/after EDTA poisoning, evaluated by EDS elemental analysis. FT-IR spectra (c) and kinetic currents @0.6 V (d) of polyCuDAB-CB in O_2-saturated 0.1 M KOH before and after EDTA.

The poison experiment was performed by stirring polyCuDAB-CB with EDTA in aqueous solution for 24 h at r.t. After centrifugation, the UV-vis spectrum of the supernatant solution was collected, which exhibited a characteristic absorption peak of Cu-EDTA complex at 271 nm (Figure S10a). The EDS elemental analysis (Figure S10b) and the FT-IR spectrum (Figure S10c) of the precipitate showed a significant decrease of Cu content and new formation of NH_2 group at 3414 cm^{-1} and 3475 cm^{-1}. These results demonstrated that Cu ions in polyCuDAB-CB were taken away via a more effective complexation by EDTA in solution. Accordingly, the EDTA poisoned polyCuDAB-CB showed a decrease of J_k (@0.6 V) by approximately 63% (Figure S10d). The more vigorous EDTA treatment (80°C, 24 h) further decrease the ORR activity with a 70% decrease of J_k (@0.6 V) (Figure 4b and S10d), indicating acceleration of the chelation at a higher temperature could further decrease the ORR activity.

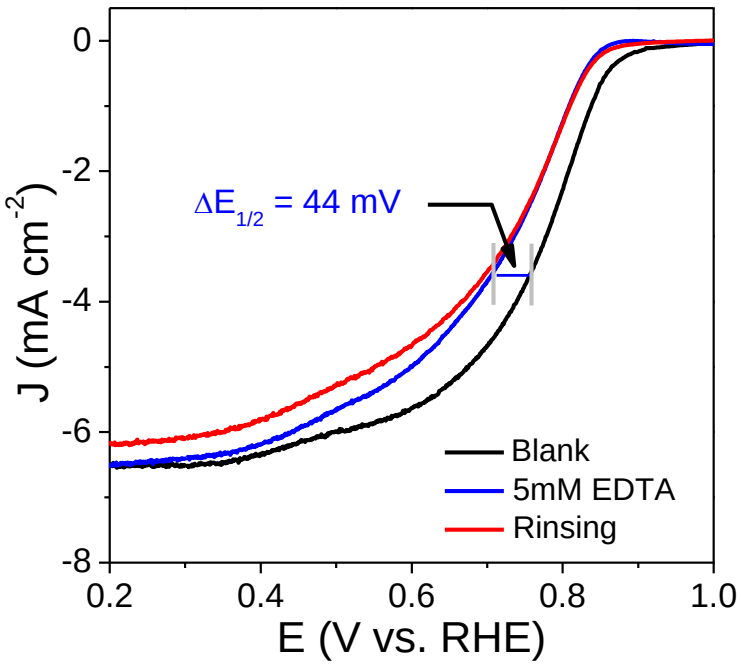

Figure S11 LSV curves of polyCuDAB-CB in O_2-saturated 0.1 M KOH without EDTA; with 5 mM EDTA; and after EDTA poisoning tests, electrode rinsing and immersion in O_2-saturated fresh 0.1 M KOH.

Directly adding 5 mM of EDTA into O_2-saturated 0.1 M KOH caused poorer E_{onset} and $E_{1/2}$ for polyCuDAB-CB, and rinsing the EDTA-poisoned polyCuDAB-CB electrode with water could not recover the ORR activity, indicative of a fast and permanent poisoning effect.

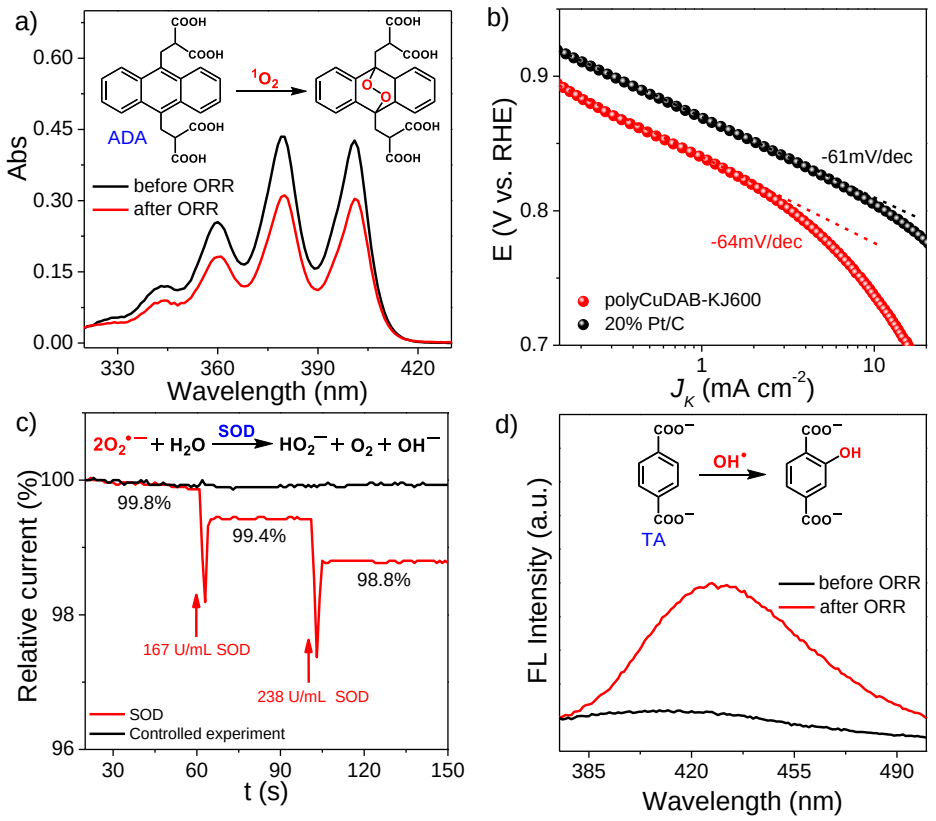

Figure S12 Trapping of the ORR intermediates for polyCuDAB-CB in ORR. (a) UV-vis absorbance decay of ADA probe caused by $^1O_2$ during ORR, suggesting that $^1O_2$ was one of ORR intermediates. (b) Tafel plots of polyCuDAB-CB and Pt/C. (c) Current-time curves on polyCuDAB-CB during ORR with and without addition of SOD, verifying the existence of $O_2^{\bullet-}$ during ORR. (d) Fluorescence spectra of TA probe to specifically verify the presence of $OH^{\bullet}$ during ORR due to hydroxylation of TA.

9, 10-anthracenediyl-bis(methylene)dimalonic acid (ADA) was firstly used as selectively trapping $^1O_2$.[2] The production of endoperoxide species led to the decrease of the UV-Vis absorption at 380 nm (Figure S12a), suggested the existence of $^1O_2$ as intermediates. Considering that the first electron transfer of ORR catalyzed by polyCuDAB-CB was the rate-determining step as indicated by the Tafel slope (-60 mV/dec, Figure S12b),[3] $O_2^{\bullet-}$ was probably involved in ORR. Such rate-determining step of the first electron transfer on polyCuDAB-CB was also confirmed by pH dependence of the redox potential of Cu(I)/Cu(II) (see more detail in Figure S13). Thus, superoxide dismutase (SOD) was chose to specifically disproportionate $O_2^{\bullet-}$.[4]

During the bulk electrolysis, successive addition of 167 U/mL and 238 U/mL SOD led to 0.4% and 0.6% decrease of ORR current (Figure S12c), respectively, essentially verifying the existence of $O_2^{\bullet -}$ during ORR. In addition, $OH^{\bullet}$ that could be probably converted from $O_2^{\bullet -}$[5] was also identified by the significant increase of the characteristic fluorescent emission of 2-hydroxyterephthalate acid at ca. 429 nm via hydroxylation of terephthalate acid (TA) during ORR (Figure S12d).

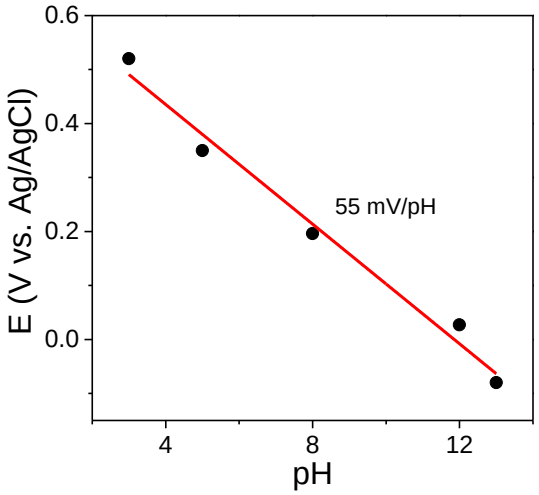

Figure S13 pH dependence of the redox potential of Cu(I)/Cu(II) for polyCuDAB-CB.

To unravel the catalytic pathway, the Cu(I)/Cu(II) redox potential of polyCuDAB-CB was further investigated over a broad range of pH (Figure S13). A slope of 55 mV/pH was observed for the variation of Cu(I)/Cu(II) redox potential towards pH, which approached to the value of 60 mV/pH predicted by the Nernst equation for a reaction involving a $1e^-/1H^+$ limiting step: Cu^{2+}-OH^- complex + H^+ + e^- → Cu^+ complex + H_2O. This was consistent with the Tafel result (Figure S12b) and the proposed mechanism (Figure 4c).

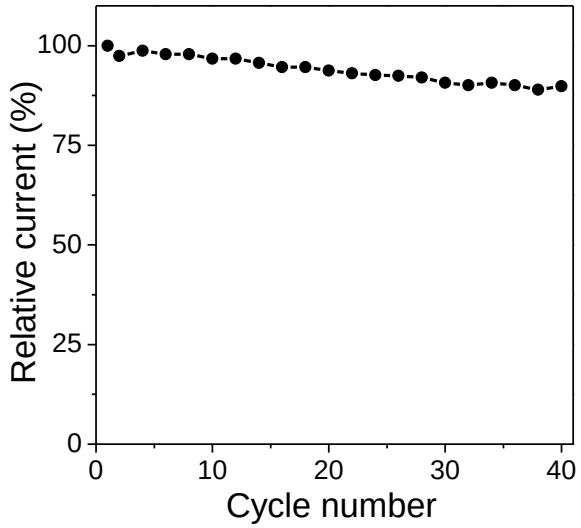

Figure S14 Plots of the relative anodic peak current versus the number of CV cycles of polyCuDAB-CB in 0.1 M KOH containing 10 mM N_2H_4, indicating the high stability of polyCuDAB-CB. Scan rate: 20 mV s^{-1}.

Table S1. Comparison of the ORR activity for the typical Cu-based catalysts in alkaline electrolyte

Catalyst	E_{onset}[a] (V vs. RHE)	$E_{1/2}$[b] (V vs. RHE)	J[c] (mA cm^{-2})	Ref.
Cu-CTF/CPs[d]	0.847	0.773	3.34	[6]
Cu@N-C[d]	0.878	0.815	4.21	[7]
nano-CuS@Cu-BTC[d]	0.861	0.723	1.95	[8]
Cu-N@C[d]	0.882	0.790	4.96	[9]
Cu-N_x/C[d]	0.845	0.729	1.69	[10]
[Cu(Hdatrz)]/C	0.824	0.730	2.04	[11]
CuO/N-rGO	0.857	0.745	2.86	[12]
CuDPA	0.758	0.615	0.35	[13]
Cu_2(N,N,N',N'-tetra(pyridine-2-ylmethyl)butane-1,4-diamine)	0.696	0.563	0.08	[13]
Cu_2(N,N,N',N'-tetra(pyridine-2-ylmethyl)hexane-1,6-diamine)	0.720	0.583	0.13	[13]
Cu_3(2,2'-([2,2'-bipyridine]-6,6'-diylbis(oxy))bis(N,N-bis(pyridin-2-ylmethyl)ethanamine))	0.681	0.554	0.07	[13]
Cu_3(2,2'-([2,2':6',2''-terpyridine]-6,6''-diylbis(oxy))bis(N,N-bis(pyridin-2-ylmethyl)ethanamine))	0.691	0.583	0.07	[13]
Pt/C	0.898	0.823	4.72	This work
polyCuDAB-CB	0.862	0.760	3.57	This work
polyCuDAB+CB	0.806	0.699	1.14	This work

[a] E_{onset} was defined as the potential at which the current density reached 5% of the diffusion-limiting current density in the cathodic scan. [b] $E_{1/2}$ was defined as the potential at which the current density reached 50% of the diffusion-limiting current density in the cathodic scan. [c] J was obtained at 0.75 V by the LSV curve. [d] Catalysts were prepared by a further high temperature pyrolysis. All potential (Eonset and $E_{1/2}$) had been converted to RHE (E(RHE)=0.196+E(Ag/AgCl)+0.059×pH).

Table S2. Comparison of the HOR activity for the typical Cu-based and many other metal-containing or high-temperature pyrolyzed catalysts

Catalyst	E_{onset}[a](V vs. RHE)	E_P[b](V vs. RHE)	Ref.
CNNs	0.861[c]	1.184[c]	[14]
RG	0.657[c]	1.068[c]	[15]
RHG	0.610[c]	1.028[c]	[15]
NHG	0.620[c]	1.045[c]	[15]
CoOEP	0.838[d]	1.047[d]	[16]
Ag/CNT	0.698[e]	0.994[e]	[17]
MnO_2-VC@Ag	0.947[c]	1.152[c]	[18]
Cu	0.742[c]	1.000[c]	[19]
CuO/C	0.992[f]	1.279[f]	[20]
Cu-GP	1.029[e]	1.208[e]	[21]
S-RGO/Cu	1.005[g]	1.268[g]	[22]
L-RGO/Cu	1.058[g]	1.340[g]	[22]
H-RGO/Cu	1.042[g]	1.293[g]	[22]
Copper (hydr)oxide	1.000[h]	1.218[h]	[23]
AuCuSn nanocubes	1.090[c]	1.218[c]	[24]
Flower-shaped CuO	0.933[g]	1.203[g]	[25]
Au-SH-SiO_2@Cu-MOF	1.174[d]	1.319[d]	[26]
Cu foil	1.058[e]	1.245[e]	This work
polyCuDAB+CB	0.647[e]	0.936[e]	This work
	0.547[e]	0.700[e]	
polyCuDAB-CB	0.566[c]	0.738[c]	This work
	0.610[g]	0.792[g]	

[a] E_{onset} was defined as the potential at which N_2H_4 began to be oxidized. [b] E_P was defined as the anodic peak potential for N_2H_4 oxidation.[21] [c] sweep rate: 20 mV s^{-1}. [d] sweep rate: 5 mV s^{-1}. [e] sweep rate: 10 mV s^{-1}. [f] sweep rate: 100 mV s^{-1}. [g] sweep rate: 50 mV s^{-1}. [h] sweep rate: 3 mV s^{-1}. All potential (E_{onset} and E_p) had been converted to RHE (E(RHE)=0.196+E(Ag/AgCl)+0.059×pH).

Supporting References

[1] X. Y. Dong, M. Zhang, R. B. Pei, Q. Wang, D. H. Wei, S. Q. Zang, Y. T. Fan, T. C. Mak, Angew. Chem. Int. Ed. 2016, 55, 2073; J. Kunze, V. Maurice, H. L. Klein, H. H. Strehblow, P. Marcus, J. Phys. Chem. B 2001, 105, 4263; J. Kunze, V. Maurice, L. H. Klein, H.-H. Strehblow, P. Marcus, Corros. Sci. 2004, 46, 245; E. Protopopoff, P. Marcus, Electrochim Acta 2005, 51, 408.

[2] R. L. Jensen, J. Arnbjerg, P. R. Ogilby, J. Am. Chem. Soc. 2012, 134, 9820; M. González-Béjar, M. Liras, L. Francés-Soriano, V. Voliani, V. Herranz-Pérez, M. Duran-Moreno, J. M. Garcia-Verdugo, E. I. Alarcon, J. C. Scaiano, J. Pérez-Prieto, J. Mater. Chem. B 2014, 2, 4554.

[3] Y. G. Li, W. Zhou, H. L. Wang, L. M. Xie, Y. Y. Liang, F. Wei, J. C. Idrobo, S. J. Pennycook, H. J. Dai, Nat. Nanotechnol. 2012, 7, 394; F. He, X. Chen, Y. Shen, Y. Li, A. Liu, S. Liu, T. Mori, Y. Zhang, J. Mater. Chem. A 2016, 4, 6630.

[4] N. He, Q. Li, D. Sun, X. Ling, Biochem. Eng. J. 2008, 38, 33; Y. Tian, L. Mao, T. Okajima, T. Ohsaka, Anal. Chem. 2002, 74, 2428; J. Di, S. Bi, M. Zhang, Biosens. Bioelectron. 2004, 19, 1479.

[5] F. Achouri, S. Corbel, A. Aboulaich, L. Balan, A. Ghrabi, M. Ben Said, R. Schneider, J. Phys. Chem. Solids 2014, 75, 1081; X. H. Qu, L. J. Kirschenbaum, E. T. Borish, Photochem. Phorobiol. 2000, 71, 307.

[6] K. Iwase, T. Yoshioka, S. Nakanishi, K. Hashimoto, K. Kamiya, Angew. Chem. Int. Ed. 2015, 54, 11068.

[7] S. H. Noh, M. H. Seo, X. Ye, Y. Makinose, T. Okajima, N. Matsushita, B. Han, T. Ohsaka, J. Mater. Chem. A 2015, 3, 22031.

[8] K. Cho, S. H. Han, M. P. Suh, Angew. Chem. Int. Ed. 2016, 55, 15301.

[9] H. Wu, H. Li, X. Zhao, Q. Liu, J. Wang, J. Xiao, S. Xie, R. Si, F. Yang, S. Miao, X. Guo, G. Wang, X. Bao, Energy Environ. Sci. 2016, 9, 3736.

[10] P. Xu, W. Chen, Q. Wang, T. Zhu, M. Wu, J. Qiao, Z. Chen, J. Zhang, RSC Adv. 2015, 5, 6195.

[11] M. Kato, K. Kimijima, M. Shibata, H. Notsu, K. Ogino, K. Inokuma, N. Ohta, H. Uehara, Y. Uemura, N. Oyaizu, T. Ohba, S. Takakusagi, K. Asakura, I. Yagi, Phys. Chem. Chem. Phys. 2015, 17, 8638.

[12] R. Zhou, Y. Zheng, D. Hulicova-Jurcakova, S. Z. Qiao, J. Mater. Chem. A 2013, 1, 13179.

[13] E. C. Tse, D. Schilter, D. L. Gray, T. B. Rauchfuss, A. A. Gewirth, Inorg. Chem. 2014, 53, 8505.

[14] R. Silva, J. Al-Sharab, T. Asefa, Angew. Chem. Int. Ed. 2012, 51, 7171.

[15] D. Yu, L. Wei, W. Jiang, H. Wang, B. Sun, Q. Zhang, K. Goh, R. Si, Y. Chen, Nanoscale 2013, 5, 3457.

[16] C. Canales, L. Gidi, R. Arce, G. Ramírez, New J. Chem. 2016, 40, 2806.

[17] G.-W. Yang, G.-Y. Gao, C. Wang, C. L. Xu, H. L. Li, Carbon 2008, 46, 747.

[18] K. J. Babu, A. Zahoor, K. S. Nahm, M. A. Aziz, P. Vengadesh, G. G. Kumar, New J. Chem. 2016, 40, 7711.

[19] K. Asazawa, K. Yamada, H. Tanaka, M. Taniguchi, K. Oguro, J. Power Sources 2009, 191, 362.

[20] Y. Ma, H. Li, R. Wang, H. Wang, W. Lv, S. Ji, J. Power Sources 2015, 289, 22.

[21] H. Gao, Y. Wang, F. Xiao, C. B. Ching, H. Duan, J. Phys. Chem. C 2012, 116, 7719.

[22] C. Liu, H. Zhang, Y. Tang, S. Luo, J. Mater. Chem. A 2014, 2, 4580.

[23] G. Karim-Nezhad, R. Jafarloo, P. S. Dorraji, Electrochim Acta 2009, 54, 5721.

[24] B. K. Patra, S. Khilari, D. Pradhan, N. Pradhan, Chem. Commun. 2016, 52, 1614.

[25] Y. Ma, H. Wang, J. Key, S. Ji, W. Lv, R. Wang, J. Power Sources 2015, 300, 344.

[26] H. Hosseini, H. Ahmar, A. Dehghani, A. Bagheri, A. R. Fakhari, M. M. Amini, Electrochim Acta 2013, 88, 301.